Chemistry–A European Journal

Research Article
doi.org/10.1002/chem.202301740

Chemistry Europe
European Chemical
Societies Publishing

www.chemeurj.org

Special Collection

Reduced Tiara-like Palladium Complex for Suzuki Cross-Coupling Reactions

Mario Daka,[a] Tiziano Montini,*[a, b] Paolo Pengo,[a] Giovanna Marussi,[a] Matteo Crosera,[a] Gianpiero Adami,[a] Juan Jose Delgado,[c, d] Giuliano Giambastiani,[e] Pierre Fertey,[f] Emiliano Fonda,[f] Lucia Pasquato,[a] and Paolo Fornasiero[a, b]

Dedicated to Professor Maurizio Prato on the occasion of his 70th birthday.

The design of highly active and structurally well-defined catalysts has become a crucial issue for heterogeneous catalysed reactions while reducing the amount of catalyst employed. Beside conventional synthetic routes, the employment of polynuclear transition metal complexes as catalysts or catalyst precursors has progressively intercepted a growing interest. These well-defined species promise to deliver catalytic systems where a strict control on the nuclearity allows to improve the catalytic performance while reducing the active phase loading. This study describes the development of a highly active and reusable palladium-based catalyst on alumina (Pd_8/Al_2O_3) for Suzuki cross-coupling reactions. An octanuclear tiara-like palladium complex was selected as active phase precursor to give isolated Pd-clusters of ca. 1 nm in size on Al_2O_3. The catalyst was thoroughly characterised by several complementary techniques to assess its structural and chemical nature. The high specific activity of the catalyst has allowed to carry out the cross-coupling reaction in 30 min using only 0.12 mol% of Pd loading under very mild and green reaction conditions. Screening of various substrates and selectivity tests, combined with recycling and benchmarking experiments, have been used to highlight the great potentialities of this new Pd_8/Al_2O_3 catalyst.

Introduction

During the last decades, transition metal nanoparticles and clusters have attracted great attention in catalysis and materials science as witnessed by the numerous studies and applications involving these nanomaterials.[1–4] Heterogeneous catalysis, in particular, has benefited of these new findings due to an increasing number of new metal based catalysts being studied at the academic level[5–7] but also with notable industrial applications.[8,9] Lately, solid phase catalysts have emerged as excellent materials in the activation of organic molecules with different degrees of complexity.[10,11]

Heterogeneous palladium catalysts based on nanoparticles (NPs) and clusters have already been employed in various chemical transformations.[12–14] During the last decades they have also been described as valuable alternatives to homogeneous palladium complexes, typically as promoters of key organic processes such as cross-coupling[15–18] and C–H bond

[a] Dr. M. Daka, Prof. Dr. T. Montini, Prof. Dr. P. Pengo, G. Marussi, Prof. Dr. M. Crosera, Prof. Dr. G. Adami, Prof. Dr. L. Pasquato, Prof. Dr. P. Fornasiero
Department of Chemical and Pharmaceutical Sciences
INSTM, UdR Trieste
University of Trieste
Trieste 34127 (Italy)
E-mail: tmontini@units.it

[b] Prof. Dr. T. Montini, Prof. Dr. P. Fornasiero
Center for Energy, Environment and
Transport Giacomo Ciamician and ICCOM-CNR Trieste Research Unit
University of Trieste
Trieste 34127 (Italy)

[c] Dr. J. J. Delgado
Departamento de Ciencia de los Materiales
Ingeniería Metalúrgica y Química Inorgánica
Universidad de Cádiz
Campus Río San Pedro, Puerto Real, Cádiz 11510 (Spain)

[d] Dr. J. J. Delgado
Instituto Universitario de Investigación en
Microscopía Electrónica y Materiales (IMEYMAT)
Universidad de Cádiz
Campus Río San Pedro, Puerto Real, Cádiz 11510 (Spain)

[e] Dr. G. Giambastiani
Institute of Chemistry of OrganoMetallic Compounds
ICCOM-CNR and Consorzio INSTM
50019 Sesto F.no, Florence (Italy)

[f] Dr. P. Fertey, Dr. E. Fonda
Synchrotron SOLEIL
L'Orme des Merisiers
Saint Aubin BP48, 91192 Gif sur Yvette Cedex (France)

Chemistry–A European Journal

Research Article
doi.org/10.1002/chem.202301740

Chemistry Europe
European Chemical
Societies Publishing

activation reactions.[19,20] Their application in cross-coupling has considerably boosted the industrial synthesis of fine chemicals, such as active pharmaceutical ingredients, natural products and advanced organic materials.[21–23] In spite of significant and technological improvements in the field, fundamental research in this area is still actively sought due to its huge impact in the evolution of synthetic organic chemistry, particularly in the terms of design and development of more efficient and sustainable catalysts and reactions set-up.

Heterogeneous palladium catalysts anchored on different supports, inorganic and/or carbonaceous, have been used in cross-coupling reactions with remarkable result.[24–29] Photocatalytic[30–33] and in-flow cross-couplings setups[34,35] have also been developed as alternative solutions to classical homogeneous protocols. Despite extensive studies on various palladium sources as well as the development of new active-phase supports, heterogeneous cross-coupling reactions catalyzed by solid-phase palladium species still suffer various issues linked to the loss of activity (*i.e.*, metal leaching) that have seriously limited the exploitation of these catalysts on a proof-of-concept ground.[36,37]

Tiara-like complexes, first reported in 1964,[38] are a class of organometallic compounds consisting in polynuclear transition metal species doubly bridged by thiolate molecules in a ring closed fashion.[38,39] These complexes are considered very promising catalysts or catalyst precursors due to a relatively small and strictly defined number of metal atoms composing the structure. Indeed, tiara-like nickel complexes have been employed as electrocatalysts, with remarkable results, for hydrogen evolution[40] and oxygen evolution reactions[41] as well as photocatalytic hydrogen evolution by water splitting.[42,43] A series of tiara-like platinum complexes have been reduced in hydrogen atmosphere affording metal clusters used in the catalytic styrene hydrogenation.[44] However, despite the great potential of these metal complexes, only a limited number of studies have been carried out on their use as catalysts, or catalyst precursors, because of their relatively low activity and the complexity in removing thiolate ligands to provide more reactive, unprotected, metal clusters.

Herein, the precise atomicity of an octanuclear tiara-like palladium complex protected by methyl thioglycolate ligands ($Pd_8(SCH_2COOMe)_{16}$) is exploited to prepare unprotected palladium clusters with a relatively narrow sized Pd NPs distribution featured by enhanced catalytic activity in the Suzuki cross-coupling reaction. The palladium complex was prepared following an already known synthetic strategy thus making use of conventional methods for the synthesis of organometallic complexes.[45] The complex was thoroughly characterised to confirm its structure before being anchored on alumina by an UV treatment and undergoing reduction at high temperature to get Pd_8/Al_2O_3 as the final species. The as-prepared Pd_8/Al_2O_3 catalyst was thoroughly characterized to determine the mean clusters size, the metal oxidation state and the catalyst composition. Afterwards, the heterogeneous system was tested for the Suzuki cross-coupling of model arylboronic acids with aryl halides under very mild experimental conditions (50 °C and 30 min reaction time) in a mixture of ethanol/water as a green

chemical environment for the process. The scope of the reaction was widely expanded using various *meta-* and *para-* substituted aryl halides to generate the corresponding substituted biphenyls which are highly valuable scaffolds for the synthesis of small molecule drugs. The Pd_8/Al_2O_3 catalyst has shown remarkable performance in the process with a very low palladium loading of 0.12 mol%. Moreover, its superior robustness and durability compared to related palladium nanoparticles/clusters of the state-of-the-art,[46] paves the way to the potential exploitation of our Pd_8/Al_2O_3 catalyst within further catalytic transformations.

Results and Discussion

Synthesis of the catalyst

Pd_8/Al_2O_3 catalyst has been prepared according to Scheme 1, following the literature procedure for the isolation of the tiara-like species $Pd_8(SCH_2COOMe)_{16}$. According to the literature, Pd thiolate complexes imply the formation of monomeric yellow coloured $Pd(SR)_2$ species[47] that, in presence of a suitable base, initiate self-condensations to give small linear oligomers forming stable ring closed complexes with an orange/red colour in solution (inset Scheme 1). The nuclearity of the final complex depends on the thiol ligand used in the complexation.

The purity of the crystalline product was confirmed by ^1H NMR[45] with the spectrum displaying two signals at 3.33 and 3.23 ppm due to the methylene groups along with two signals at 3.96 and 3.77 ppm due to the methoxy fragments (Figure S1). These two sets of signals are attributed to the axial and equatorial methoxycarbonylmethylene arms of the cyclic complex. This assignment is consistent with previous NMR characterizations of related species, such as the cyclic hexameric Pd thiolate complexes.[48,49] Furthermore, a comparative single crystal X-ray diffraction analysis carried out on isolated complex crystals (Figure S2) allowed to confirm its ultimate nature (Table S1).[45] The crystallised complex was then deposited onto Al_2O_3 through an irradiation/deposition process using UV light (Figure 1A). The deposition was accomplished with the aim at preparing a catalyst with a nominal Pd loading of 0.2 wt.%. The exact amount of the Pd-active phase was confirmed afterwards by Inductively Coupled Plasma – Optical Emission Spectroscopy
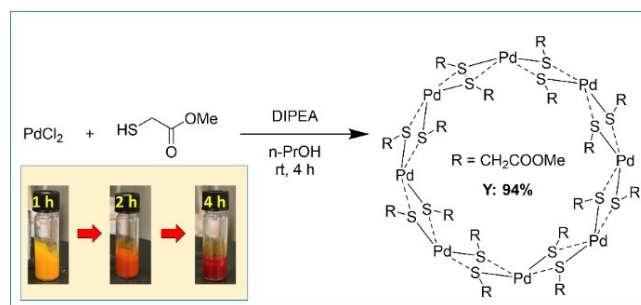
Scheme 1. Synthetic scheme for the $Pd_8(SCH_2COOMe)_{16}$ complex preparation and colour progression of the reaction (inset).

Chemistry–A European Journal

Research Article
doi.org/10.1002/chem.202301740

Chemistry Europe
European Chemical
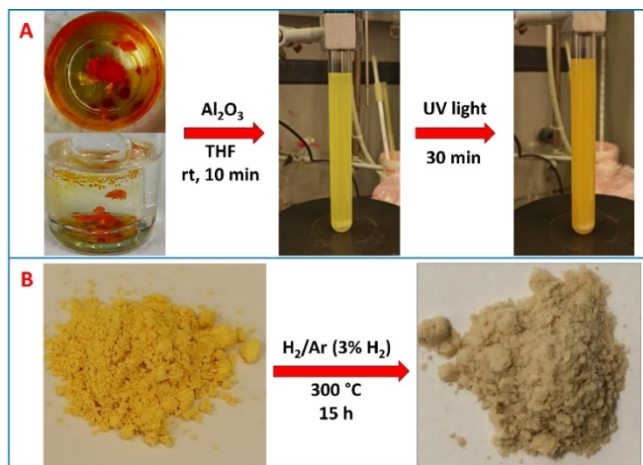Societies Publishing

Figure 1. Representative images of the irradiation/deposition process (A) and reduction step performed in H_2/Ar on the pre-reduced catalyst (B).

(ICP-OES) analysis and it was fixed in the 0.13–0.17 wt.% (see Experimental section). It is already known that thiols and sulfides can undergo radical sulfur-carbon bond cleavage under UV light.[50] This reactivity was then exploited to prepare PdS clusters from the $Pd_8(SCH_2COOMe)_{16}$ complex upon UV irradiation, followed by its adsorption on alumina by ion-dipole interaction. Without UV irradiation, the thiolate complex failed to adsorb on the support because of the hydrophobicity imparted by the organic ligands. Moreover, we found that the choice of the support was pivotal in avoiding aggregation of the palladium species during deposition, with Al_2O_3 being identified as the optimal choice. After UV irradiation, a slight colour change of both the suspension and the alumina was observed (Figure 1A). The last step in the preparation of the catalyst consisted in the reduction of the Al_2O_3-adsorbed PdS clusters under H_2 atmosphere. Mild temperature conditions have been selected for this stage as to limit the occurrence of sintering phenomena of the Pd-active phase, hence maximizing the advantage of the utilization of well-defined molecular precursors in the preparation of narrowed sized Pd-clusters. The pre-catalyst, after being dried under vacuum, was finely crushed and treated in a H_2/Ar flow at 300 °C for 15 h to afford a grey brownish powder hereinafter referred to as Pd_8/Al_2O_3 (Figure 1B).

Catalyst characterization

To confirm the effective removal of the organic ligands during all the sample treatments, infrared (IR) analysis was performed on both the UV-irradiated and reduced catalyst (Figure S3). IR spectra confirmed that $Pd_8(SCH_2COOMe)_{16}$ adsorbed on Al_2O_3 in a molecular form. UV irradiation resulted in the removal of C–H bond while reduction at 300 °C under H_2 atmosphere completed the removal of residual organic moieties from the precursor.

X-ray photoelectron spectroscopy (XPS) analyses was carried out on the catalyst to investigate the evolution of Pd and S

during the preparation path. Survey spectra for the UV-irradiated and reduced catalysts are shown in Figure S4. The Pd 3d spectrum typically falls in the 325 to 350 eV energy region but its very low content hampered a clear signal detection in the survey spectra. High resolution XPS spectra on the UV-irradiated catalyst (Figure 2A) display signatures (336.3 eV, $3d^{5/2}$; 341.6 eV, $3d^{3/2}$) that are typical of Pd^{2+} suggesting its presence in the form of palladium sulfide. This was also confirmed by the analysis on sulfur. Indeed, XPS spectra display binding energies at 164.0 eV ($2p^{3/2}$) and 164.0 eV ($2p^{1/2}$) that are consistent with the presence of PdS.[51] As expected, the spectra of the Pd_8/Al_2O_3 catalyst after reduction treatment in H_2 (Figure 2B) highlight the presence of metallic Pd (335.6 eV, $3d^{5/2}$; 341.1 eV, $3d^{3/2}$) while sulfur appears below the detection limit, suggesting the removal of sulfur ligands to a larger extent.

X-ray Absorption Fine Structure (XAFS) measurements have additionally been performed on catalysts and pre-catalysts [$Pd_8(SCH_2COOMe)_{16}$ complex, $Pd_8(SCH_2COOMe)_{16}$ impregnated on Al_2O_3, UV-irradiated and the reduced catalyst (Pd_8/Al_2O_3)] as to get more insights on the Pd coordination environment. The obtained results are reported in Figure 3A, 3B and Table S2. As expected, for the $Pd_8(SCH_2COOMe)_{16}$ complex only Pd–S was observed in the first coordination shell: fixing the coordination number (CN) to 4, a distance of 0.2328 nm is obtained, which was in good agreement with the average Pd–S bond length determined from single crystal structure of the tiara-like complex. The same values were obtained also for the impregnated complex, confirming the retention of the $Pd_8(SCH_2COOMe)_{16}$ molecular structure after adsorption on the support.
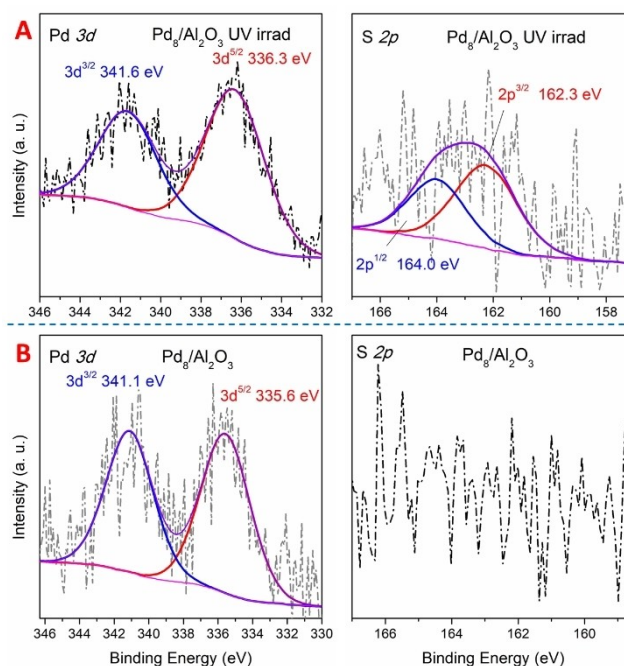

Figure 2. High resolution XPS spectra for the UV-irradiated catalyst (A) and the reduced Pd_8/Al_2O_3 (B) in the Pd and S binding energies ranges.

Chemistry–A European Journal

Research Article
doi.org/10.1002/chem.202301740

Chemistry
Europe
European Chemical
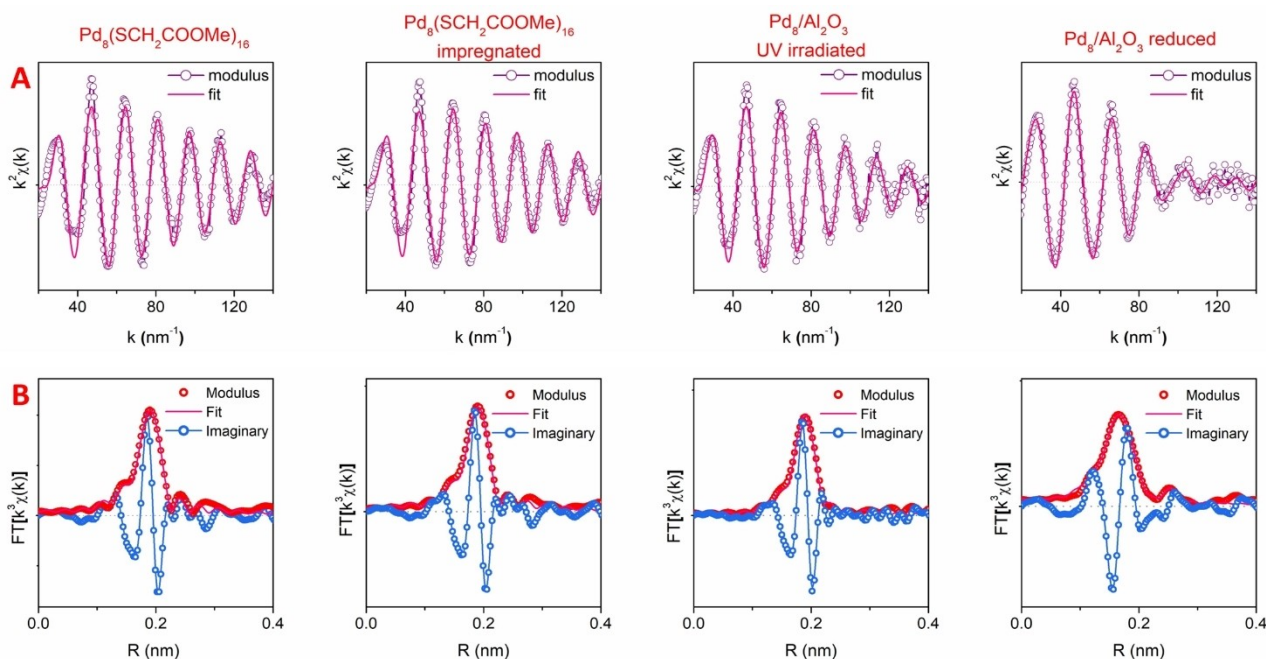Societies Publishing

Figure 3. Fitted EXAFS (A) and Fourier transform (B) spectra of the Pd species recorded at various stages of the preparation.

The pre-catalyst after the UV irradiation process still displays the presence of sulphur bound to palladium although at a slightly reduced distance (0.2313 nm). This suggests a small reassessment of the Pd clusters on the alumina support after the cleavage of the organic chains. A marked change in the Pd environment was instead observed after the reduction of the catalyst in H_2 atmosphere. Pd–S contribution to Extended XAFS (EXAFS) signal strongly decreases, showing a CN=0.9 and suggesting the removal of S from the material, in agreement with XPS analysis. Pd–O and Pd–Pd distances also appear in the fitting of EXAFS data. The Pd–O presence was related to the interaction of Pd clusters with the oxygen atoms of the support (CN=2.1). However, the presence of palladium oxide cannot be excluded as the absorption of oxygen increases while decreasing the size of Pd NCs. Most notably, the low CN for Pd–Pd (0.2) is a clear indication of the small size of the metal clusters that remain anchored to the Al_2O_3 surface after the pre-catalyst reduction.

To confirm these results, samples obtained after organic fragments removal have been analysed by High-angle annular dark-field Scanning Transmission Electron Microscopy (HAADF-STEM) to evaluate the size and composition of Pd clusters (Figure 4). The representative STEM images of the UV-irradiated and reduced Pd_8/Al_2O_3 samples show that alumina particles are composed of crystallites of 10–20 nm, with well-defined shapes and high crystallinity (Figure 4A and 4D). Together with large Al_2O_3 particles, a few small particles can be observed as brighter spots with size around 1–2 nm (Figure 4B and 4D). The Energy-dispersive X-ray Spectroscopy (EDS) analysis on these particles shows a weak, but clear, signal related to Pd, indicating that the bright spots represent the Pd-containing clusters derived from the $Pd_8(SCH_2COOMe)_{16}$ complex (Figure 4C and 4F). Notably,
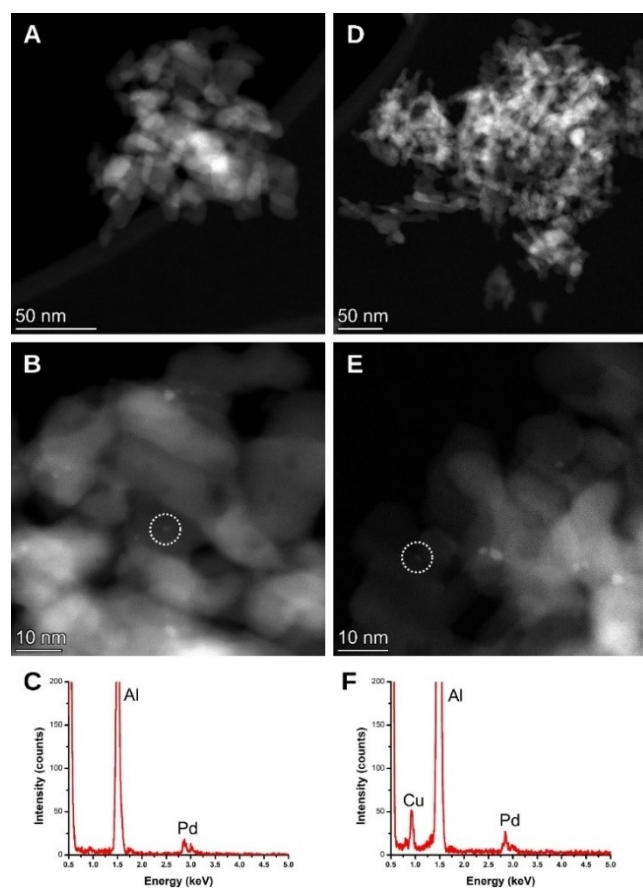

Figure 4. Representative images from HAADF-STEM characterization of the UV irradiated (left) and reduced (right) Pd_8/Al_2O_3 materials: general view (A, D), high magnification images (B, E), EDS analysis of the bright spots (C, F).

Chemistry–A European Journal

Research Article
doi.org/10.1002/chem.202301740

Chemistry Europe
European Chemical
Societies Publishing

EDS signal is quite low and always present with intense signals from Al and O deriving from the support. It must be underlined that, in both the cases, the signal for S is not clearly detectable due to the very low amount under the electron beam.

Before testing the Pd_8/Al_2O_3 catalyst, its textural properties have been investigated by physisorption analysis. The N_2 physisorption isotherms reported in Figure S5 indicate that no significant changes to textural properties of the materials take place after deposition of $Pd_8(SCH_2COOMe)_{16}$ complex, UV irradiation and H_2 reduction, showing high surface area and pore volume (Table S3) comparable to those of pristine Al_2O_3 calcined at 900 °C. Hysteresis loops and BJH analysis show, for all the samples, the presence of an extensive mesoporous system with a maximum of pore size distribution centred at 28 nm (Figure S6).
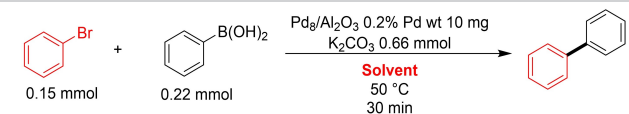
Suzuki cross-coupling reactions

The investigation of Pd_8/Al_2O_3 activity in the Suzuki cross-coupling required a preliminary optimization of the reaction conditions with reference to a detailed screening of the solvent, base, temperature and reaction time. The coupling of bromobenzene with phenylboronic acid was selected as the model reaction. A target temperature value of 50 °C for 30 min of reaction time were fixed as starting operative conditions while screening the nature of solvent and base. Initially, K_2CO_3 was used as a reference base for the solvent screening.

As displayed in Table 1, the use of water as solvent resulted into poor reactants conversion. Although water is generally considered as a good solvent for the dispersion stability of supported catalysts, the limited solubility of organic reactants together with their moderate diffusion towards the catalytic sites gave very poor conversions only. On the other hand, pure alcohols such as EtOH and MeOH provided cross-coupling products only in moderate yield (40.7 % and 24.3 % respectively). Notably, the use of water/ethanol mixture (1 : 1 v/v) resulted in a very high yield (>99 %) towards the biphenyl product. The high miscibility of the two solvents resulted in a synergistic and positive combination of their solvent effects.[52] The use of other organic solvents resulted again in very low yields; in particular, using THF, 1,4-dioxane or DMSO resulted in negligible reactants conversions only.
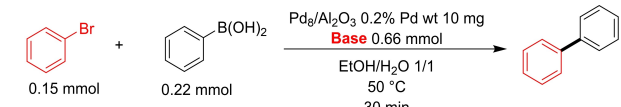
After the optimal solvent mixture was identified, different inorganic and organic bases were screened (Table 2). Inorganic bases were screened displaying from poor to discrete conversion yields. With respect to K_2CO_3, other related inorganics salts such as Cs_2CO_3 and Na_2CO_3 gave acceptable yields, 40.7 % and 60.4 % respectively, while phosphates, K_3PO_4 and Na_3PO_4, performed slightly worse. The superior yield obtained with carbonate bases can be ascribed to their suitable properties in shifting the acid-base equilibrium between organoboronic acid and organoborate toward the second one which is the real partner in the transmetalation with palladium. In addition, a counterion effect can be attributed to K^+ for the proper stabilization of the $R-B(OH)_3^-$ organoborate species.[53] On the other hand, low activity was observed with the use of bicarbonates and hydroxides with conversions laying on moderate values comprises between 11.1 % and 15 %. Similarly, organic bases, such as amines gave poor or very low product yields. Hence, K_2CO_3 resulted the best performing base for the process allowing to achieve almost quantitative reagents conversion.

Table 1. Solvents screening for the optimisation of the Suzuki coupling.

Pd_8/Al_2O_3 0.2% Pd wt 10 mg
K_2CO_3 0.66 mmol
Solvent
50 °C
30 min

Bromobenzene 0.15 mmol + phenylboronic acid $B(OH)_2$ 0.22 mmol → biphenyl

Entry	Solvent	Yield [%][a]
1	H_2O	4.5
2	EtOH	40.7
3	MeOH	24.3
4	**EtOH/H_2O 1/1**	**>99**
5	MeCN	2.7
6	THF	traces
7	1,4-dioxane	traces
8	Acetone	2.2
9	Toluene	7.7
10	DMF	2.5
11	DMSO	traces

[a] Based on the biphenyl product and determined by GC-MS with benzophenone as internal standard.

Table 2. Screening of different bases for the optimization of the Suzuki coupling.

Pd_8/Al_2O_3 0.2% Pd wt 10 mg
Base 0.66 mmol
EtOH/H_2O 1/1
50 °C
30 min

Bromobenzene 0.15 mmol + phenylboronic acid $B(OH)_2$ 0.22 mmol → biphenyl

Entry	Base	Yield [%][a]
1	none	0
2	**K_2CO_3**	**>99**
3	Cs_2CO_3	40.7
4	Na_2CO_3	60.4
5	$KHCO_3$	11.1
6	$NaHCO_3$	11.6
7	K_3PO_4	43.4
8	Na_3PO_4	24.9
9	KOH	12.3
10	NaOH	15
11	DMAP	traces
12	DABCO	34.6
13	DIPEA	7.3
14	TEA	13

[a] Based on the biphenyl product and determined by GC-MS with benzophenone as internal standard.

Chemistry–A European Journal

Research Article
doi.org/10.1002/chem.202301740

Chemistry
Europe

European Chemical
Societies Publishing

Attempts to further optimize the reaction conditions gave no significant improvements with respect to the initial set-up. Reactions performed at room temperature (25 °C) resulted in lower yields down to 43.9% within the same reaction time. A similar trend was also observed when the reaction time was reduced from 30 min to 20 min. A conversion yield of 75% was recorded while maintaining all other experimental parameters unchanged. After these considerations, the temperature of 50 °C and reaction time of 30 min were kept as optimal parameters for running the cross-coupling reactions efficiently. A last screening test was performed under inert atmosphere (Ar) which delivered a 70% yield in product. This result was in agreement with literature data suggesting a rate enhancement in the presence of oxygen when using solid palladium. Oxygen favours PdO formation, which has higher solubility in aqueous media, thus favouring highly active Pd ionic species in solution.[52] The selectivity of the reaction was assessed by means of model homocoupling experiments. These catalytic tests were performed using one of the two reactants only for getting the coupling product: bromobenzene or phenylboronic acid (Scheme S1). At the optimised reaction conditions, bromobenzene afforded the homocoupling product only in traces while phenylboronic acid gave biphenyl with 2.2% conversion. These results suggest a very high selectivity of the catalyst in promoting only the cross-coupling reaction with a high discrimination towards the homocoupling side product. To support the high activity of the Pd_8/Al_2O_3 catalyst at this low Pd loading, a crucial control experiment was also performed. Along the years various studies have reported metal-free cross-coupling reactions that were afterwards recognised to be the result of data misinterpretation.[54–56] It is well known that cross-coupling reactions need a metal catalyst to proceed and when the metal is not provided on purpose, alleged metal-free cross-coupling reactions take place as the result of metal contaminants in the reagents.

In order to rule out the presence of possible palladium contaminations in the reactants or in the base, a catalytic test was additionally performed employing the bare Al_2O_3 support without the Pd_8 clusters. As expected, the test failed pointing out no conversion of reactants into cross-coupling products and hence attributing the observed catalytic activity to the Pd_8/Al_2O_3 catalyst only. Furthermore, to highlight the importance of the reduction step in delivering an active catalyst, a test was performed with the UV irradiated material: in this case GC-MS analysis of the crude reaction mixture allowed to determine a negligible 4% yield of biphenyl.

The scope of the reaction was expanded to a series of substituted bromoarenes to give the corresponding products as illustrated in Scheme 2. The yields refer to isolated products after purification of the crude mixture by flash chromatography. Para-substituted bromoarenes were mostly employed because of their availability, while ortho-substituted bromoarenes were not considered for the scope: a preliminary test on 2-bromobenzaldehyde gave only traces of the product. Concerning the functional group (FG) tolerance, the catalyst behaved remarkably well, displaying to be suitable for cross-coupling reactions on substrates bearing functional groups of different
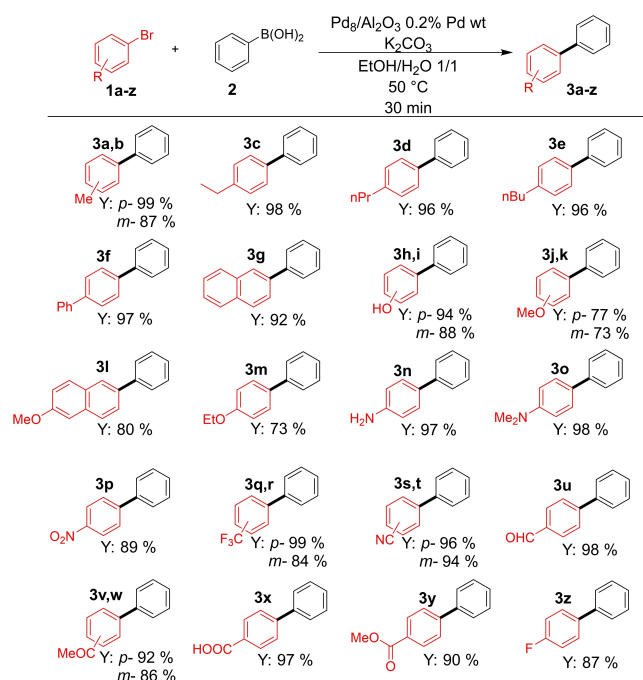
Scheme 2. Reaction scope on substituted bromoarenes (reaction conditions: Pd_8/Al_2O_3 10 mg, bromoarene 0.15 mmol, phenylboronic acid 0.22 mmol, K_2CO_3 0.66 mmol, $H_2O/EtOH$ 1/1 2 mL, 50 °C, 30 min).

nature. Alkyl FGs were well tolerated in the catalysis providing the corresponding products **3a**–**3e** from excellent to quantitative yield (from 87% to 99%). Aromatic substituents on the bromoarene gave products **3f** and **3g** in high yield while the biphenyl product from the coupling of 2-bromo-6-methoxynaphtalene and phenylboronic acid (**3l**) was isolated in 80% yield. Hydroxy and methoxy FGs both in meta and para also resulted in the expected products **3h**, **3i** and **3j**, **3k**, respectively, with good yield while bromoaniline derivatives delivered products **3n** and **3o** in quantitative yield. Remarkably, bromoarenes containing electron-withdrawing groups displayed good reactivity although they are known to reduce the kinetics of the oxidative addition step in Pd catalysed cross-coupling reactions. Bromoarenes with electron-withdrawing FGs gave products in high to remarkably high yield such as 4-trifluoromethylbiphenyl **3q** (99%), 4-phenylbenzonitrile **3s** (96%), 4-phenylbenzaldehyde **3u** (98%) or 4-biphenylcarboxylic acid **3x** (97%). Overall, the catalyst demonstrated its excellent performance in the process by promoting the cross-coupling process in combination with several different meta- and para-substituted substrates under mild experimental conditions.

Additional tests were carried out to compare the performance of Pd_8/Al_2O_3 with respect to classical systems of the state-of-the-art such as the commercial Pd/C 10% and Pd/Al_2O_3 prepared by impregnation/reduction of K_2PdCl_4 (0.2 wt.% Pd) following the same conditions applied to the preparation of Pd_8/Al_2O_3. All comparative catalytic tests were performed with 0.12 mol% of Pd whatever the nature of the selected catalyst at work and results are summarised on Table 3. The commercial Pd/C displayed only moderate activity (7.4% conversion) toward

Chem. Eur. J. **2023**, *29*, e202301740 (6 of 10)

© 2023 The Authors. Chemistry - A European Journal published by Wiley-VCH GmbH

Chemistry–A European Journal

Research Article
doi.org/10.1002/chem.202301740

**Chemistry
Europe**
European Chemical
Societies Publishing

Table 3. Activity benchmarking with a commercial Pd catalyst and a lab standard Pd/Al_2O_3 using 0.12 mol% of Pd.

Entry	Catalyst	Yield [%][a]
1	Pd$_8$/Al$_2$O$_3$ 0.2 % wt	> 99
2	Pd/C 10 % wt	7.4
3	Pd/Al$_2$O$_3$ 0.2 % wt	24

[a] Based on the biphenyl product and determined by GC-MS with benzophenone as internal standard.

the Suzuki coupling under the same experimental conditions used with Pd$_8$/Al$_2$O$_3$; the benchmark Pd/Al$_2$O$_3$ afforded up to 24% yield which was higher with respect to Pd/C but still not comparable with that of the Pd$_8$/Al$_2$O$_3$. Additional comparative outcomes of Pd$_8$/Al$_2$O$_3$ with other related systems from the literature are summarised in Table S4 for the sake of completeness.

To properly assess the usefulness of a heterogeneous catalyst and to better estimate its potentialities, reusability and robustness tests are mandatory. It is widely accepted that cross-coupling reactions promoted by solid phase palladium species proceeds through a cocktail-type mechanism.[57] This latter based on the dissolution and re-deposition of active species such as single atoms, clusters and NPs. Therefore, the overall catalyst performance needs to be assessed in the light of its ability to control the occurrence of metal atoms agglomeration during the re-deposition step. Recycling tests can offer useful hints on the stability of the catalytic material. Catalytic data reported in Figure 5 present the conversion yield to biphenyl in the cross-coupling of bromobenzene and phenylboronic acid
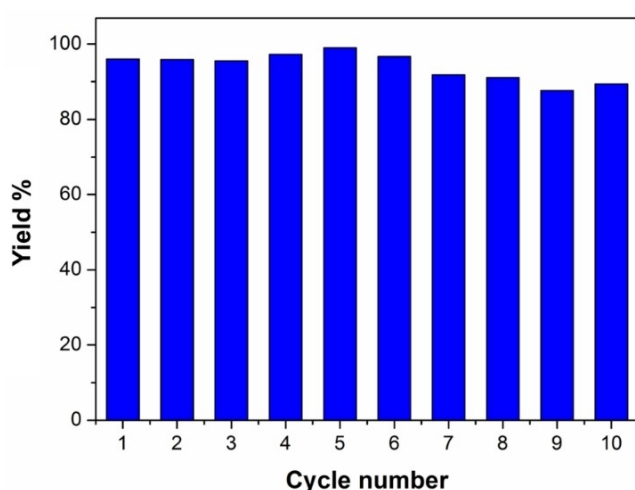
promoted by Pd$_8$/Al$_2$O$_3$ recycled within 10 consecutive experiments. The ability of the catalyst in promoting the reaction with high yield (between 96% and 99%) was maintained almost unchanged within six consecutive catalytic runs. Afterwards, conversion decreased slightly down to 87% and 89% for the 9th and 10th recycling test, respectively. It can be inferred that the high activity maintained throughout many recycling runs is the consequence of a negligible leaching of the catalyst active phase. This was corroborated by ICP-OES analysis of the reaction medium after filtration. The analysis showed a Pd concentration lower the limit of detection (LOD) of the instrument (10 ppb). This amount corresponds roughly to a maximum value of 0.5% of the total number of Pd atoms introduced into the reaction vial. This fraction is not negligible but, considering that the Pd signal cannot be distinguished from the signal noise, it is reasonable to assume that the leached Pd at the end of the catalytic process was in a limited amount.

Nevertheless, EXAFS analysis of the Pd$_8$/Al$_2$O$_3$, after the 1st and 10th recycling (Figure S7, Table S5) has unveiled a significant agglomeration of the Pd active phase in the successively re-used catalyst. The data obtained for the recovered catalyst after the 1st recycle showed a minor increase of the Pd–Pd CN (2.8) and of the Pd–S CN (2.7) accompanied by a decrease of the Pd–O CN (0.4). After 10th recycling runs, the Pd–Pd CN increased to 6.5, Pd–S CN reduced to 1.1 and the Pd–O contribution disappeared, suggesting the presence of bigger clusters/particles. In accordance with these spectroscopic evidence, HAADF-STEM characterization of the sample after the 1st recycling test showed the presence of aggregates of Pd-containing particles (Figure S8A and S8B). EDS mapping clearly revealed the concomitance of Pd and S signals (Figure S8C and S8D). After the 10th recycling test, larger particles were observed (Figure S9A and S9B), with EDS mapping confirming the concomitance of Pd and S. Notably, the EDS mapping (Figure S9C and S9D) of the used catalyst has shown the appearance of a clear peak related to K, as a residue of the base (K$_2$CO$_3$) employed throughout the catalytic tests.

All these data taken together support the fast dissolution of Pd species in the reaction media followed by their re-deposition as metallic Pd to deliver supported clusters on Al$_2$O$_3$ without compromising the overall catalyst activity in a longer period of use.

Conclusions

In conclusion, a palladium polynuclear complex was exploited for the design of a highly active and robust solid phase catalyst for Suzuki cross-couplings. Catalyst and pre-catalyst were thoroughly characterized by different techniques throughout all preparation steps. Electron microscopy analyses gave insight on the dispersion of palladium clusters on the Al$_2$O$_3$ support, while XPS and EXAFS investigations contributed to determining the composition and structural evolution of the palladium clusters. The high activity and selectivity of the isolated Pd$_8$/Al$_2$O$_3$ catalyst were assessed by extensive tests and control experiments. The performance of Pd$_8$/Al$_2$O$_3$ has allowed to widen the

Figure 5. Recycling tests for the Pd$_8$/Al$_2$O$_3$ catalyst used in the Suzuki cross-coupling reaction (reaction conditions: Pd$_8$/Al$_2$O$_3$ 10 mg, bromoarene 0.15 mmol, phenylboronic acid 0.22 mmol, K$_2$CO$_3$ 0.66 mmol, H$_2$O/EtOH 1/1 2 mL, 50 °C, 30 min).

Chemistry–A European Journal

Research Article
doi.org/10.1002/chem.202301740

**Chemistry
Europe**
European Chemical
Societies Publishing

scope of the reaction by including several bromoarenes bearing electron-withdrawing and electron-donating substituents, hence demonstrating the flexibility of this catalyst at work. All tested substrates were converted to the corresponding substituted biphenyls in excellent yields, under very mild reaction conditions and with the use of green solvents mixture. The superior performance of the Pd_8/Al_2O_3 in the process was confirmed by comparing it with benchmark Pd/Al_2O_3 systems of the *state-of-the-art*. Lastly, the stability of Pd_8/Al_2O_3 was evaluated by repeated recycling tests (up to 10 successive reuse), during which cross-coupling conversions systematically ranked to high values. This study based on Suzuki cross-coupling reactions illustrates the potentialities of this new Pd catalyst obtained from a polynuclear tiara-like complex. Overall, the new procedure described in the paper to the preparation of solid phase catalysts featured by a narrow distribution of small metal clusters, contributes to add new insights and solutions towards the design of well-defined supported metal clusters and their successive employment in green catalytic processes.

Experimental Section

Materials: All reagents employed were supplied by Merck and Alfa Aesar and used without purification, unless where indicated. Solvents were purchased from Merck and VWR. Deuterated solvents were bought from Merck and Cambridge Isotope Laboratories. Al_2O_3 Puralox TH100/150 was supplied by Sasol. Reactions were monitored by TLC on Merck silica gel plates (0.25 mm) and visualized by UV light, $KMnO_4$ stain or $Ce_2(MoO_4)_3$ stain solutions. Flash chromatography was performed on Normasil silica gel 60® 40–63 µm purchased from VWR. All the glassware employed for the preparation of the materials and for the catalytic tests was cleaned with aqua regia (HCl/HNO_3 3/1 v/v) and rinsed with MilliQ water before use.

Synthesis of the tiara-like complex $Pd_8(SCH_2COOMe)_{16}$: The synthesis of the tiara-like complex $Pd_8(SCH_2COOMe)_{16}$ was performed following the literature precedents and described hereafter for the sake of completeness.[45] Briefly, $PdCl_2$ (50 mg, 0.28 mmol) was firstly finely dispersed in 0.5 mL *n*-propanol with the aid of a sonication bath for 5 min. The as-obtained $PdCl_2$ dispersion was added dropwise, at room temperature, to a 4 mL scintillation screw capped glass vial, equipped with stirring bar, containing a 0.5 mL *n*-propanol solution prepared by using 51 µL of methyl thioglycolate (0.57 mmol) and 96 µL *N,N*-diisopropylethylamine (DIPEA) (0.56 mmol). The reaction mixture was vigorously stirred at room temperature for 4 h before being filtered on a Gooch funnel with a type IV porosity frit. The yellow solid obtained from the filtration was thoroughly washed with methanol directly on the funnel to remove the excess thiol and DIPEA. The $Pd_8(SCH_2COOMe)_{16}$ complex was finally collected off the frit with DCM and it was finally crystallised by diffusion of *n*-pentane vapours in DCM at 4 °C for 3 days. Orange-yellow plate shaped crystals and their aggregates in lumps were obtained in 94% yield on Pd basis (84 mg, 0.033 mmol). ^1H NMR (400 MHz, $CDCl_3$) δ (ppm): 3.96 (s, 24 H), 3.77 (s, 24 H), 3.33 (s, 16 H), 3.23 (s, 16 H).

$Pd_8(SCH_2COOMe)_{16}$ irradiation/deposition over Al_2O_3: The deposition of the $Pd_8(SCH_2COOME)_{16}$ complex was performed as described hereafter: Alumina (100 mg) was firstly dispersed in 17 mL of inhibitor free THF with the aid of a sonication bath for 10 min and vigorously stirred in a 20 mL screw-capped tube-shaped vial. Subsequently, 1 mg of $Pd_8(SCH_2COOMe)_{16}$ dissolved in 3 mL THF

was added dropwise to the suspension and stirred for 10 min further. The amount of Pd complex to be deposited was fixed in order to achieve a final 0.2 wt.% Pd loading. The suspension was then irradiated with UV light (450 W halogen lamp) for 30 min under stirring to decompose the ligands and favour the adsorption of Pd–S clusters onto the support. After irradiation, the suspension was filtered on a 0.45 µm PVDF filter disk and the solid material was dried at 60 °C under vacuum overnight. The as-obtained precatalyst was finely crushed to get a tiny powder before undergoing any further treatment.

Reduction to Pd_8/Al_2O_3: The dried pre-catalyst was introduced in a tube-shaped quartz reactor equipped with a quartz inlet tube, screw-sealed together between rubber gaskets, and connected to H_2/Ar gas line. The reactor was then purged with Ar gas for 30 min and placed in a pit furnace where it was heated at 300 °C (5 °C min⁻¹ ramp) for 15 h under H_2/Ar flow (3% H_2, 100 mL min⁻¹). After this reduction step, the catalyst was collected for characterization and catalytic tests. The powder was stored in glass vials in air atmosphere. The exact amount of Pd-loading was determined afterwards via ICP-OES analysis.

Synthesis of benchmark catalyst Pd/Al_2O_3 0.2 wt.%: A benchmark Pd/Al_2O_3 catalyst was prepared by impregnation of a commercially available palladium salt to the support followed by reduction under the same conditions outlined above for Pd_8/Al_2O_3. Briefly, 1 g of Al_2O_3 was dispersed in 200 mL H_2O in a 250 mL round bottom flask and stirred vigorously. To the suspension, a freshly prepared K_2PdCl_4 (6.1 mg) solution in 10 mL H_2O was added dropwise and left to stir for 12 h. The suspension was then centrifuged at 6000 rpm for 10 min and dried in vacuum at 60 °C overnight. The as-obtained pre-catalyst was finely crushed in a mortar and reduced in a tube-shaped quartz reactor at 300 °C (5 °C min⁻¹ ramp) for 15 h under H_2/Ar flow (3% H_2, 100 mL min⁻¹). As for the Pd_8/Al_2O_3 catalyst, the exact Pd-loading was fixed afterwards via ICP-OES analysis.

Suzuki cross-coupling reaction: Unless otherwise stated, all catalytic tests were performed under air atmosphere as follows: 10 mg Pd_8/Al_2O_3 (0.2% Pd wt), arylboronic acid (0.22 mmol) and K_2CO_3 (0.66 mmol) were introduced in a 10 mL screw-capped tube-shaped vial, equipped with a stirring bar. Subsequently, 2 mL ethanol/water (1/1 v/v ratio) were added and stirred at room temperature. After 2 min, aryl halide (0.15 mmol) was added to the reaction mixture, the vial was sealed and placed in a preheated water bath at 50 °C for 30 min under vigorous stirring. After 30 min the vial was cooled to room temperature and the solution extracted with EtOAc (2×5 mL). The organic extracts were washed with water (5 mL) and brine (10 mL) before being dried over Na_2SO_4. After filtration and solvent removal, the product was purified by flash chromatography in *n*-Hex/EtOAc to yield the desired product. Reactions were analysed by quantitative GC-MS using a calibration curve with internal standard (benzophenone). All reaction crude products were analysed prior to extraction and purification steps.

Characterization: For TEM analysis, a small amount of the dry catalyst powders was deposited onto a holey carbon film supported on a 300-mesh nickel grid. The samples were then characterized using high-resolution transmission electron microscopy (HRTEM) and scanning transmission electron microscopy-high angle annular dark field (STEM-HAADF) with a Talos F200X instrument. The STEM-HAADF technique is highly sensitive to the atomic number of the elements, with the intensity roughly proportional to the square of the atomic number (Z^2), allowing for the distinction of small nanoparticles supported on lighter materials. Additionally, elemental mapping was performed using energy dispersive X-ray spectroscopy (EDX) to investigate the distribution of elements. EDX mappings were acquired with a beam current of 200 pA and a

Chemistry–A European Journal

Research Article
doi.org/10.1002/chem.202301740

Chemistry Europe
European Chemical
Societies Publishing

dwell time of 128 µs per pixel. To enhance the visual quality of the obtained elemental maps, a Gaussian blur filter with a value of 0.8 was applied using Velox software. The images were analysed using ImageJ 1.52a software.

Inductively Coupled Plasma-Optical Emission Spectroscopy (ICP-OES) analyses were performed using an Optima 8000 Spectrometer equipped with a S10 autosampler (PerkinElmer, USA). All the catalyst samples were previously treated with aqua regia solution (1 mL) for 3 h to dissolve the palladium clusters, afterwards, the same solution was diluted 1:10 and filtered on PTFE 0.22 µm filter disk to remove undissolved Al_2O_3. The total palladium concentration was quantified after instrument calibration, performed by diluting the multistandard solution for ICP analysis (Periodic Table MIX2, Merck). All standards (range: 0–10.0 mg/L) were prepared by acidifying to 10% with aqua regia to compensate for the matrix effect. The limit of detection at the operative wavelength (340.458 nm) was 0.05 mg/L. The precision of the measurements expressed as repeatability (as RSD%) for the analysis was always less than 5%.

Textural properties were analysed by N_2 physisorption at liquid nitrogen temperature using a Micrometrics ASAP 2020 automatic analyser. All the NPs were degassed at 300 °C for 12 h at 10 µmHg. The specific surface area was obtained by applying the Brunauer–Emmett–Teller (BET) method equation. Pore size distribution was determined applying the Barrett, Joyner, Halenda (BJH) method equation to the desorption branch of the isotherms.

The X-ray photoelectron spectroscopy (XPS) measurements were performed in an ultrahigh vacuum (UHV) spectrometer equipped with a RESOLVE 120 MCD5 hemispherical electron analyser. The Al Kα hν = 1486.6 eV dual anode X-ray source was used as incident radiation. The constant pass energy mode was used to record both survey and high-resolution spectra, with pass energies 100 and 20 eV, respectively.

Single crystal XRD data were recorded at the CRISTAL beamline at SOLEIL synchrotron using a monochromatic beam (40×40 µm²) with an energy of 18466 eV. A Rayonix SX165 detector was employed to acquire reflection in the range $1.354 < \theta < 38.666$. During acquisition of the data, the single crystal of $Pd_8(SCH_2COOMe)_{16}$ was maintained at low temperature with a flow of N_2 from evaporation from liquid nitrogen.

X-ray absorption spectra (named here µX both for normalized linear absorption coefficient or fluorescence yield), in the near edge (XANES) and extended (EXAFS) energy ranges, were measured at the SAMBA beamline of Synchrotron SOLEIL. Ex-situ samples were mixed with transparent BN powder and formed into pellets for the analysis. Spectra of samples at the Pd K edge were collected by measuring the Kα emission of Pd with a pixelated (6×6) Ge detector (Mirion) with DxMap digital signal processors (XIA). Dead time correction was applied on the basis of the calibrated estimate from DxpMap DSP cards by XIA Ltd. Data on standard materials were measured in transmission mode. EXAFS data analysis was carried out with theoretical standards from Feff 8.455 and with the Demeter software for data handling (Athena) and fitting (Artemis). All fits were carried out in R-space ($30 \leq k \leq 140$ nm^{-1}; $0.125 \leq r \leq 0.30$ nm; EXAFS data have been k^2 weighted). The amplitude reduction factor (S_0^2) was estimated by fitting the EXAFS signal of a Pd metallic foil and its value was fixed to 0.875.

IR spectra were recorded in attenuated total reflectance (ATR) mode on a Shimadzu IRAffinity-1S spectrophotometer equipped with a QATR 10 accessory.

Nuclear magnetic resonance (NMR) spectra were recorded on a Varian 400 spectrometer operating at 400 MHz for proton. The NMR spectra have been processed by means of MestReNova software. ^1H NMR spectra were referenced to the residual protons in the deuterated solvent. ^{13}C NMR spectra were referenced to the solvent chemical shift. Chemical shifts (δ) are reported in ppm and the multiplicity of each signal is identified by the conventional abbreviations: s for singlet, d for doublet, t for triplet, q for quartet, dd for doublet of doublets, dt for doublet of triplets, m for multiplet, br for broad peak. Coupling constants (J) are reported in Hertz (Hz).

GC-MS analyses were performed on an Agilent 7890 GC gas chromatograph equipped with an Agilent 5975 C mass spectrometer and mounting a J&D DB-225 m column (60 m, 0.25 mm ID, 0.25 µm film) and using He as carrier. The conversion percentage in the catalytic tests was determined by interpolation of the product and internals standard peak area ratios in a calibration curve built with standard concentrations of biphenyl and benzophenone.

Supporting Information

The Supporting Information includes single crystal XRD, IR, EXAFS, XPS, physisorption data, NMR data. The authors have cited additional references within the Supporting Information (Ref. [24,58–78]):

Conflict of Interests

The authors declare no conflict of interest.

Data Availability Statement

The data that support the findings of this study are available from the corresponding author upon reasonable request.

Keywords: EXAFS · HAADF-STEM · heterogeneous catalysis · irradiation/deposition process · low loading Pd catalysts

[1] T. Sun, Y. S. Zhang, B. Pang, D. C. Hyun, M. Yang, Y. Xia, *Angew. Chem. Int. Ed.* **2014**, *53*, 12320–12364.

[2] E. Ozbay, *Science* **2006**, *311*, 189–193.

[3] A. K. Yetisen, H. Qu, A. Manbachi, H. Butt, M. R. Dokmeci, J. P. Hinestroza, M. Skorobogatiy, A. Khademhosseini, S. H. Yun, *ACS Nano* **2016**, *10*, 3042–3068.

[4] Y. Du, H. Sheng, D. Astruc, M. Zhu, *Chem. Rev.* **2020**, *120*, 526–622.

Chemistry–A European Journal

Research Article
doi.org/10.1002/chem.202301740

Chemistry Europe
European Chemical
Societies Publishing

[5] Z. Li, S. Ji, Y. Liu, X. Cao, S. Tian, Y. Chen, Z. Niu, Y. Li, *Chem. Rev.* **2020**, *120*, 623–682.

[6] T. Montini, M. Melchionna, M. Monai, P. Fornasiero, *Chem. Rev.* **2016**, *116*, 5987–6041.

[7] K. D. Gilroy, A. Ruditskiy, H. C. Peng, D. Qin, Y. Xia, *Chem. Rev.* **2016**, *116*, 10414–10472.

[8] W. J. Stark, P. R. Stoessel, W. Wohlleben, A. Hafner, *Chem. Soc. Rev.* **2015**, *44*, 5793–5805.

[9] M. Schmal, *Heterogeneous Catalysis and Its Industrial Applications*, Springer Cham, **2016**, p. 373.

[10] L. Yin, J. Liebscher, *Chem. Rev.* **2007**, *107*, 133–173.

[11] N. K. Ojha, G. v. Zyryanov, A. Majee, V. N. Charushin, O. N. Chupakhin, S. Santra, *Coord. Chem. Rev.* **2017**, *353*, 1–57.

[12] M. Cargnello, N. L. Wieder, T. Montini, R. J. Gorte, P. Fornasiero, *J. Am. Chem. Soc.* **2010**, *132*, 1402–1409.

[13] M. Cargnello, J. J. Delgado Jaén, J. C. Hernández Garrido, K. Bakhmutsky, T. Montini, J. J. Calvino Gámez, R. J. Gorte, P. Fornasiero, *Science* **2012**, *337*, 713–717.

[14] M. Cargnello, V. V. T. Doan-Nguyen, T. R. Gordon, R. E. Diaz, E. A. Stach, R. J. Gorte, P. Fornasiero, C. B. Murray, *Science* **2013**, *341*, 771–773.

[15] I. Favier, D. Pla, M. Gómez, *Chem. Rev.* **2020**, *120*, 1146–1183.

[16] A. Balanta, C. Godard, C. Claver, *Chem. Soc. Rev.* **2011**, *40*, 4973–4985.

[17] F. Amoroso, S. Colussi, A. Del Zotto, J. Llorca, A. Trovarelli, *Catal. Lett.* **2013**, *143*, 547–554.

[18] A. Del Zotto, S. Colussi, A. Trovarelli, *Inorg. Chim. Acta* **2018**, *470*, 275–283.

[19] J. M. Asensio, D. Bouzouita, P. W. N. M. van Leeuwen, B. Chaudret, *Chem. Rev.* **2020**, *120*, 1042–1084.

[20] S. Vásquez-Céspedes, K. M. Chepiga, N. Möller, A. H. Schäfer, F. Glorius, *ACS Catal.* **2016**, *6*, 5954–5961.

[21] C. Torborg, M. Beller, *Adv. Synth. Catal.* **2009**, *351*, 3027–3043.

[22] T. Banno, Y. Hayakawa, M. Umeno, *J. Organomet. Chem.* **2002**, *653*, 288–291.

[23] J.-P. Corbet, G. Mignani, *Chem. Rev.* **2006**, *106*, 2651–2710.

[24] J. Sun, Y. Fu, G. He, X. Sun, X. Wang, *Appl. Catal. B* **2015**, *165*, 661–667.

[25] X. Tao, R. Long, D. Wu, Y. Hu, G. Qiu, Z. Qi, B. Li, R. Jiang, Y. Xiong, *Small* **2020**, *16*, 1–11.

[26] C. Yue, Q. Xing, P. Sun, Z. Zhao, H. Lv, F. Li, *Nat. Commun.* **2021**, *12*, 1–14.

[27] B. M. Choudary, S. Madhi, N. S. Chowdari, M. L. Kantam, B. Sreedhar, *J. Am. Chem. Soc.* **2002**, *124*, 14127–14136.

[28] M. Gao, J. Wang, W. Shang, Y. Chai, W. Dai, G. Wu, N. Guan, L. Li, *Catal. Today* **2022**, *410*, 237–246.

[29] F. Amoroso, S. Colussi, A. Del Zotto, J. Llorca, A. Trovarelli, *J. Mol. Catal. A-Chem.* **2010**, *315*, 197–204.

[30] Y. Huang, S. Yang, M. Jiang, J. Li, L. Peng, C. Cao, W. Song, *Cryst. Growth Des.* **2020**, *20*, 7526–7532.

[31] Q. Xiao, S. Sarina, A. Bo, J. Jia, H. Liu, D. P. Arnold, Y. Huang, H. Wu, H. Zhu, *ACS Catal.* **2014**, *4*, 1725–1734.

[32] F. Raza, D. Yim, J. H. Park, H. I. Kim, S. J. Jeon, J. H. Kim, *J. Am. Chem. Soc.* **2017**, *139*, 14767–14774.

[33] S. Zhang, C. Chang, Z. Huang, Y. Ma, W. Gao, J. Li, Y. Qu, *ACS Catal.* **2015**, *5*, 6481–6488.

[34] F. Ferlin, S. Santoro, L. Ackermann, L. Vaccaro, *Green Chem.* **2017**, *19*, 2510–2514.

[35] Z. Chen, E. Vorobyeva, S. Mitchell, E. Fako, M. A. Ortuño, N. López, S. M. Collins, P. A. Midgley, S. Richard, G. Vilé, J. Pérez-Ramírez, *Nat. Nanotechnol.* **2018**, *13*, 702–707.

[36] D. B. Eremin, V. P. Ananikov, *Coord. Chem. Rev.* **2017**, *346*, 2–19.

[37] S. S. Soomro, F. L. Ansari, K. Chatziapostolou, K. Köhler, *J. Catal.* **2010**, *273*, 138–146.

[38] R. G. Hayter, F. S. Humiec, *J. Inorg. Nucl. Chem.* **1964**, *26*, 807–810.

[39] P. Woodward, L. F. Dahl, E. W. Abel, B. C. Crosse, *J. Am. Chem. Soc.* **1965**, *87*, 5251–5253.

[40] R. Angamuthu, E. Bouwman, *Phys. Chem. Chem. Phys.* **2009**, *11*, 5578–5583.

[41] D. R. Kauffman, D. Alfonso, D. N. Tafen, J. Lekse, C. Wang, X. Deng, J. Lee, H. Jang, J. S. Lee, S. Kumar, C. Matranga, *ACS Catal.* **2016**, *6*, 1225–1234.

[42] W. Zhang, J. Hong, J. Zheng, Z. Huang, J. (Steve) Zhou, R. Xu, *J. Am. Chem. Soc.* **2011**, *133*, 20680–20683.

[43] H. N. Kagalwala, E. Gottlieb, G. Li, T. Li, R. Jin, S. Bernhard, *Inorg. Chem.* **2013**, *52*, 9094–9101.

[44] T. Imaoka, Y. Akanuma, N. Haruta, S. Tsuchiya, K. Ishihara, T. Okayasu, W. J. Chun, M. Takahashi, K. Yamamoto, *Nat. Commun.* **2017**, *8*, 1–8.

[45] Y. Yamashina, Y. Kataoka, Y. Ura, *Inorg. Chem.* **2014**, *53*, 3558–3567.

[46] M. Díaz-Sánchez, D. Díaz-García, S. Prashar, S. Gómez-Ruiz, *Environ. Chem. Lett.* **2019**, *17*, 1585–1602.

[47] J. Chen, L. Liu, L. Weng, Y. Lin, L. Liao, C. Wang, J. Yang, Z. Wu, *Sci. Rep.* **2015**, *5*, 4–11.

[48] Z. Yang, A. B. Smetana, C. M. Sorensen, K. J. Klabunde, *Inorg. Chem.* **2007**, *46*, 2427–2431.

[49] V. P. Ananikov, N. v. Orlov, S. S. Zalesskiy, I. P. Beletskaya, V. N. Khrustalev, D. G. Musaev, *J. Am. Chem. Soc.* **2012**, *134*, 6637–6649.

[50] S. M. Bonesi, M. Fagnoni, D. Dondi, A. Albini, *Inorg. Chim. Acta* **2007**, *360*, 1230–1234.

[51] C. Du, P. Li, F. Yang, G. Cheng, S. Chen, W. Luo, *ACS Appl. Mater. Interfaces* **2018**, *10*, 753–761.

[52] F. Amoroso, S. Colussi, A. Del Zotto, J. Llorca, A. Trovarelli, *Catal. Commun.* **2011**, *12*, 563–567.

[53] C. F. R. A. C. Lima, A. S. M. C. Rodrigues, V. L. M. Silva, A. M. S. Silva, L. M. N. B. F. Santos, *ChemCatChem* **2014**, *6*, 1291–1302.

[54] Z. Novák, R. Adamik, J. T. Csenki, F. Béke, R. Gavaldik, B. Varga, B. Nagy, Z. May, J. Daru, Z. Gonda, G. L. Tolnai, *Nat. Catal.* **2021**, *4*, 991–993.

[55] W. Liu, H. Cao, H. Zhang, H. Zhang, K. H. Chung, C. He, H. Wang, F. Y. Kwong, A. Lei, *J. Am. Chem. Soc.* **2010**, *132*, 16737–16740.

[56] N. E. Leadbeater, M. Marco, *J. Org. Chem.* **2003**, *68*, 5660–5667.

[57] V. P. Ananikov, I. P. Beletskaya, *Organometallics* **2012**, *31*, 1595–1604.

[58] P. Wang, J. Cai, J. Chen, M. Ji, *J. Braz. Chem. Soc.* **2015**, *26*, 748–754.

[59] P. Mondal, P. Bhanja, R. Khatun, A. Bhaumik, D. Das, S. Manirul Islam, *J. Colloid Interface Sci.* **2017**, *508*, 378–386.

[60] K. Martina, F. Baricco, M. Caporaso, G. Berlier, G. Cravotto, *ChemCatChem* **2016**, *8*, 1176–1184.

[61] S. R. Borhade, S. B. Waghmode, *Beilstein J. Org. Chem.* **2011**, *7*, 310–319.

[62] L. Mohammadi, M. Hosseinifard, M. R. Vaezi, *ACS Omega* **2023**, *8*, 8505–8518.

[63] F. Shukla, M. Patel, Q. Gulamnabi, S. Thakore, *Dalton Trans.* **2023**, *52*, 2518–2532.

[64] S. S. Qin, Z. K. Wang, L. Hu, X. H. Du, Z. Wu, M. Strømme, Q. F. Zhang, C. Xu, *Nanoscale* **2021**, *13*, 3967–3973.

[65] Y. Li, H. Zhong, Y. Jin, B. Guan, J. Yue, R. Zhao, Y. Huang, *ACS Appl. Mater. Interfaces* **2022**, *14*, 40408–40417.

[66] L. Bai, J. X. Wang, *Adv. Synth. Catal.* **2008**, *350*, 315–320.

[67] I. Fujii, K. Semba, Y. Nakao, *Org. Lett.* **2022**, *24*, 3075–3079.

[68] B. Karimi, D. Elhamifar, J. H. Clark, A. J. Hunt, *Chem. Eur. J.* **2010**, *16*, 8047–8053.

[69] M. Jiang, L. P. Liu, M. Shi, Y. Li, *Org. Lett.* **2010**, *12*, 116–119.

[70] A. Tsubouchi, D. Muramatsu, T. Takeda, *Angew. Chem. Int. Ed.* **2013**, *52*, 12719–12722.

[71] G. M. Scheuermann, L. Rumi, P. Steurer, W. Bannwarth, R. Mülhaupt, *J. Am. Chem. Soc.* **2009**, *131*, 8262–8270.

[72] S. Shi, G. Meng, M. Szostak, *Angew. Chem. Int. Ed.* **2016**, *55*, 6959–6963.

[73] M. H. Savanur, R. G. Kalkhambkar, K. K. Laali, *Appl. Catal. A-Gen.* **2017**, *543*, 150–161.

[74] E. Salanouve, G. Bouzemame, S. Blanchard, E. Derat, M. Desage-El Murr, L. Fensterbank, *Chem. Eur. J.* **2014**, *20*, 4754–4761.

[75] G. A. Molander, S. L. J. Trice, S. M. Kennedy, *J. Org. Chem.* **2012**, *77*, 8678–8688.

[76] F. Khosravi, M. Gholinejad, D. Lledó, G. Grindlay, C. Nájera, J. M. Sansano, *J. Organomet. Chem.* **2019**, *901*, 120941.

[77] A. Mercadante, V. Campisciano, A. Morena, L. Valentino, V. La Parola, C. Aprile, M. Gruttadauria, F. Giacalone, *Eur. J. Org. Chem.* **2022**, *2022*, e202200497.

[78] H. G. Ghalehshahi, R. Madsen, *Chem. Eur. J.* **2017**, *23*, 11920–11926.